

Modelling the growth stress in tree branches: eccentric growth *vs.* reaction wood

A. Van Rooij^{1,2}, E. Badel², J.F. Barczi³, Y. Caraglio³, T. Alméras⁴ and J. Gril^{1,2}

1. Université Clermont-Auvergne, CNRS, Institut Pascal, F-63000, Clermont-Ferrand, France

2. Université Clermont-Auvergne, INRAE, PIAF, F-63000, Clermont-Ferrand, France

3. CIRAD, UMR AMAP, F-34398 Montpellier, France.

AMAP, Univ Montpellier, CIRAD, CNRS, INRAE, IRD, Montpellier, France.

4. LMGC, CNRS, Université of Montpellier, Montpellier, France

Abstract

This work aims to model the mechanical processes used by tree branches to control their posture despite their increasing weight loading. The two known options for a branch to maintain its orientation are the asymmetry of maturation stress, including reaction wood formation, and eccentric radial growth. Both options can be observed in nature and influence the stress distribution developed in the branch each year. This so-called "growth stress" reflects the mechanical state of the branch. In this work, a growth stress model was developed at the cross-section level in order to quantify and study the bio-mechanical impact of each process. For illustration, this model was applied to branches of two 50-year-old trees, one softwood *Pinus pinaster* and one hardwood *Prunus avium* (wild cherry tree), both simulated with the AmapSim discrete element software. For the wild cherry tree, the computed outputs enlightened that the eccentricity of radial growth seems to be as efficient as the formation of reaction wood to maintain the postural control despite the increasing gravity.^{err} ~~The computed outputs enlightened that, for both *Prunus avium* and *Pinus pinaster*, eccentric radial growth appears less efficient than the formation of reaction wood to counter the increasing gravity stress applied to the branch.~~^{err} For the pine tree, eccentric radial growth appears to be less efficient than the formation of reaction wood^{err}. But although ~~eccentric growth~~^{err} it^{err} does not necessarily act as a relevant lever for postural control, it greatly modifies the profile pattern of mechanical stress and could provide mechanical safety of the branch. This work opens experimental perspectives to understand the biomechanical processes involved in the formation of branches and their mechanical safety.

28 Abbreviations and notations (in order of occurrence)

NW, TW, CW	Normal Wood, Tension Wood, Compression Wood
(x, y, z)	Local reference coordinates associated with the section
O	Centre of the section
r, R	Radial polar coordinate and Radii of the cross section (m)
$e(R), \bar{e}(R)$	Eccentricity at the stem radius R, integrated eccentricity up to $r = R$
(x', y', z')	Local reference coordinates associated with the section, centred on the pith
σ	Stress (MPa)
σ_0	Induced maturation stress (Mpa)
S	Cross section area (m^2)
N, M	Loads (N): normal force parallel to z' and bending moment around y'
E	Module of elasticity in L direction (GPa): MOE
μ	Induced maturation strain
ϵ, a, b	Strain, at the center, local curvature
K_i	Structural stiffness of the cross-section
F_i	External coefficients (maturation and load)
θ	Circumferential position in section (rad)
$\sigma_0(\theta)$	Maturation strain in the new ring at circumferential position θ
α	Mean maturation stress in the new ring
β	Differential stress in the new ring
$R_{x'y'}$	Radius of the cross section at the instant of appearance of the point (x', y')
$\lambda_N, \lambda_M, \nu_M, \nu_N$	Load power law: allometric coefficient
λ_b, ν_b	Change of curvature power law: allometric coefficient
$\sigma_{NW}, \sigma_{TW}, \sigma_{CW}$	Maturation stress in the normal wood, tension wood and compression wood
$\mu_{NW}, \mu_{TW}, \mu_{CW}$	Maturation strain in the normal wood, tension wood and compression wood
\vec{N}_n, \vec{M}_n	Loads of growth unit n: normal force and bending moment around y
N_z, M_x, M_y, M_z	Loads of growth unit n: projection of \vec{N}_n on \vec{z} and bending moment \vec{M}_n around $\vec{x}, \vec{y}, \vec{z}$
m_n	Mass of the growth unit n (kg)
g	Gravity constant: $g = 9.8 \text{ m.s}^{-2}$
G_n	Centre of gravity of the growth unit n
E_d, E_g	Air-dry, green MOE
ρ	Density
μstrain	$1/10^6$
D_n, D_{n+1}	First and second diameter the growth unit n
D_f	Deflection of a growth unit
L_n	Length of the growth unit n

31 Introduction

32 From a mechanical point of view, wood in trees fulfils three major functions: construction of the tree
33 structure, postural control of trunk and branches and breaking resistance to external stimuli [Thibaut
34 (2019)]. These three functions are provided by the way wood cells differentiate and accumulate during
35 the wood formation process. Each axis of a tree can be considered as an inclined beam, consisting of
36 a succession of conical growth units [Barthélémy and Caraglio (2007)]. It is built in two steps: first,
37 primary growth resulting in new growth units that increase the length of the initial axis; and secondary
38 growth resulting in thickening of already existing units by addition of annual rings. These two interactive
39 and additional processes lead to a specific pattern of mechanical stress, called 'growth stress', which can
40 be analysed as the superposition of support stress and maturation stress [Archer (1976); Fournier et al.

(1991a)]. The support stress results from the continuous increase of the weight supported by the axis over the years. It reaches maximal levels close to the stem and vanishes near stem periphery, where the recently formed wood contributes to the support of recently produced biomass only. Maturation stress is set up at the end of the cell-wall maturation process, when molecular components such as lignin polymerise, generating growth forces by small dilatation or contraction restrained by the rigidity of the previously formed wood cells [Alméras and Clair (2016)]. An evaluation of the maturation stress can be obtained by measuring the strain associated to stress release at stem periphery, where no support stress is present [Nicholson (1971); Yoshida and Okuyama: (2002); Yang et al. (2005)]. The circumferential heterogeneity of this peripheral stress is needed to regulate stem curvature. In most cases, a tensile maturation stress is produced in the newly formed 'normal wood'. But observations on inclined trunks [Alméras et al. (2005); Coutand et al. (2007); Thibaut and Gril (2021)], seedlings [Hung et al. (2016)] and branches [Fisher and Stevenson (1981); Huang et al. (2010); Tsai et al. (2012); Hung et al. (2017)] have evidenced a clear difference between hardwood and softwood **behaviour**. Hardwoods ~~are able to~~ produce 'tension wood' (**TW**), inducing a much higher tensile stress on one side, while for softwood, a compressive stress is induced in 'compression wood' (**CW**). The first pulls, the second pushes. In the most usual case of inclined stems restoring their vertical orientation, **tension wood TW** is formed on the upper side while **compression wood CW** is formed on the lower side of the trunk. But other situations can be encountered depending on the biomechanical requirements of the tree [Wang et al. (2009b)]. In addition to their participation in the postural control of tree stems, these two types of so-called 'reaction wood' (**RW**) are characterised by specific anatomical pattern (not discussed here) and specific physical and mechanical properties.

As an alternative to complex experimental approaches, growth stress modelling plays an important role in the understanding of the phenomena involved in the orientation process of a stem. The history of biomechanical models began with Kübler (1959) who proposed an analytical formulation of growth stress for a perfect cylinder made of a homogeneous and transversally isotropic wood. Later, Archer and Byrnes (1974) took into account an asymmetry of the maturation stress, and Fournier et al. (1991a,b) proposed a semi-incremental version of these models, allowing to take into account a potential gradient of mechanical parameters (stiffness, maturation).

By associating their previous model to the loading induced by the tree weight, Fournier et al. (1994) made the connection between growth stress and stem orientation. This model has been adopted and developed by several authors in order to study the orientation process of stems. Yamamoto et al. (2002) added a primary shoot and returned to curvature calculations. Alméras and Fournier (2009) introduced the notion of gravitropic performance (capacity of the tree to correct the bending moment induced by its weight) and proposed criteria of long-term stability. Huang et al. (2005) and Alméras et al. (2005) improved the model by introducing a secondary growth asymmetry and its resulting pith eccentricity, as well as stiffness heterogeneity, allowing to quantify the effectiveness of eccentricity, maturation, stiffness gradient and initial radius in the curvature regulation process. They ~~highlighted enlightened~~ that the main factor in the gravitropic process is the spatial distribution of the maturation stress. Still in line with Fournier's 1994 model, Alméras et al. (2018) recently developed analytical models of longitudinal growth stress, taking into account different configurations, like eccentricity or maturation gradient, and evolution laws, like evolution of stiffness per additional layer. Finally, based on the same philosophy as established by Kübler, tree-scale and finite-element models have emerged [Fourcaud et al. (2003); Ancelin et al. (2004)].

Huang et al. (2010)'s model has been used to understand how eccentric growth and **reaction wood RW** are involved in branch orientation [Wang et al. (2009a); Huang et al. (2010); Tsai et al. (2012); Hung et al. (2017)], but all these studies were based on the current state of the branch, without consideration of the previous history: although some of them quantified the roles of maturation and eccentricity in the regulation of curvature, none did evaluate their capacity to ensure a given growth scenario.

Unlike trunks, which usually seek verticality, after the first stages of growth, branches tend to grow in a stationary way at a fixed angle to the vertical. Therefore, in this framework, we focus on understanding

90 how branches can control their orientation, through the study of two growth parameters: eccentric growth
91 and [compression wood CW](#). The aim is to check by calculation what option is mechanically possible and
92 safe for the branch. For this purpose, we developed a semi-incremental biomechanical model of growth
93 stress at the cross section level that takes into account the eccentricity and maturation gradients during the
94 construction of branches. Using the digital models of [a softwood \(*Pinus pinaster* Aiton\)](#) and [a hardwood](#)
95 [\(*Prunus avium* L\)](#) ~~one softwood *Pinus pinaster* and one hardwood *Prunus avium*~~, the impact of each of
96 these two growth parameters on the stress state was evaluated.

97 **Material and methods**

98 **Numerical model**

99 **General hypotheses**

100 The problem was set in the framework of the beam theory. From a geometrical point of view, branches
101 generally show profiles that suit to this type of analytical framework: a slender shape and no important
102 diameter variations. The shape effects due to twigs and other local biological phenomena (cavity, nodes,
103 etc.) were neglected. The same set of hypotheses as in Alm eras et al. (2018) was adopted. In this study,
104 we focused on the behaviour in the longitudinal direction (parallel to the main axis). Horizontal bending
105 and torsion loads were not considered. Only the vertical bending moment (caused by the weight) was
106 considered; these hypotheses on the loading modes are discussed later.

107 **Geometrical settings**

108 The object of study was the cross-section of a branch, placed within a plane locally orthogonal to the pith.
109 The local reference frame of the section is $(\vec{x}, \vec{y}, \vec{z})$, with \vec{z} the longitudinal direction of the axis, and \vec{x}
110 placed in a vertical plane and facing upwards (Fig 1). The shape of the cross-section was assumed to be
111 circular at any stage of development, described by the successive depositions of wood rings. The term of
112 'ring' refers here to the volume occupied by wood cells produced by the cambium during a certain duration
113 of time, not necessarily annual: it must be taken in a numerical meaning. These rings possibly could
114 present an eccentricity resulting from asymmetry of secondary growth. Since the model only takes into
115 account vertical bending, the eccentricity was set along the x axis, as expressed by the following equation:

$$O(t) = \int_0^{R(t)} e(r) dr = \bar{e}R(t) \quad (1)$$

116 with $O(t)$ the position of the geometrical centre and $R(t)$ the radius of the section at time t , $e(r)$ the
117 eccentricity when the stem radius was r and \bar{e} the integrated eccentricity up to $r = R$. The eccentricity can
118 vary in the interval $[-1, 1]$. A zero eccentricity corresponds to a centred section, while -1 or 1 corresponds
119 to maximum eccentricity resulting from secondary growth only on the lower or the upper side of the
120 section, respectively. In the following, the position x' in the pith reference frame is needed. By calling x
121 the vertical position in the geometrical reference frame, we deduce from equation (1):

$$x = x' - \bar{e}R \quad (2)$$

122 **Computation of the mechanical behaviour**

123 We developed a radial incremental method. For each radial increment, the longitudinal stress was computed
124 in order to satisfy the static equilibrium of the cross section:

$$\begin{cases} \int_S \delta\sigma dS + \int_{\delta S} \sigma_0 dS = \delta N & (3a) \\ \int_S \delta\sigma x dS + \int_{\delta S} \sigma_0 x dS = -\delta M & (3b) \end{cases}$$

125 where S is the cross-section area, δS is its increment, $\delta\sigma$ is the increment of stress σ in the already formed
 126 wood, in response to the maturation stress σ_0 generated in the new wood layer. δN and δM are respectively
 127 the increment of external force N and bending moment M , that are applied on the cross-section. For
 128 illustration, the geometric situation for K rings and an increment of stem radius δR is proposed in Fig 1.

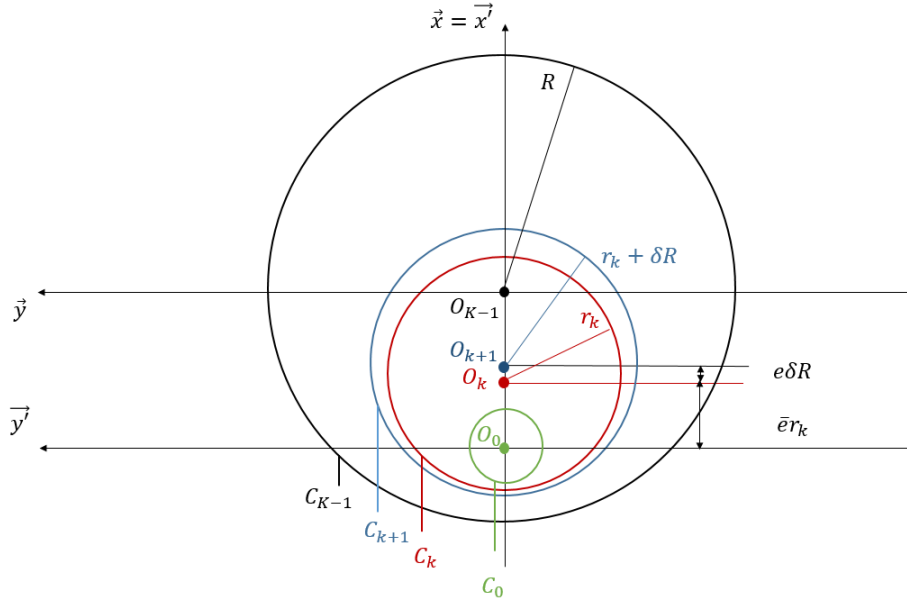


Figure 1: Geometrical representation of a section with K numerical rings and a radial increment δR between rings $(k - 1)$ and k .

129

130 The stress σ is linked to the strain ϵ by a classical pre-stressed Hooke's law:

$$\sigma = E (\epsilon - \mu) = E\epsilon + \sigma_0 \quad (4)$$

131 where E is the longitudinal Young's modulus, μ is the maturation strain and σ_0 is the maturation stress.
 132 In the context of the beam theory, the planar cross-sections remain so (Euler-Bernoulli assumption). The
 133 strain field is then described by the deformation a at the centre of the pith and the curvature b relative to
 134 the y -axis, as follows:

$$\delta\epsilon = \delta a + x\delta b \quad (5)$$

135 where $\delta\epsilon$, δa , δb are the increments of ϵ , a , b , respectively. The stress increment $\delta\sigma$, in the already formed
 136 wood, where no maturation occurs anymore, can then be deduced:

$$\delta\sigma = E\delta\epsilon = E(\delta a + x\delta b) \quad (6)$$

From these considerations, the system (3) becomes (details of the calculation are given in Appendix A):

$$\begin{cases} K_0\delta a + K_1\delta b = \delta F_0 & (7a) \\ K_1\delta a + K_2\delta b = \delta F_1 & (7b) \end{cases}$$

137 with

$$K_0 = E\pi R^2, \quad K_1 = E\pi\bar{e}R^3, \quad K_2 = E\pi R^4 \left(\bar{e}^2 + \frac{1}{4} \right) \quad (8)$$

$$\delta F_0 = - \int_{\delta S} \sigma_0 dS + \delta N, \quad \delta F_1 = - \int_{\delta S} \sigma_0 x dS - \delta M$$

138 The calculation of the coefficients δF_0 and δF_1 depends on the formulation of the maturation stress. The
139 maturation stress was assumed to vary circumferentially as follows:

$$\sigma_0(\theta) = \alpha + \beta \cos \theta \quad (9)$$

where the mean stress α and differential stress β were defined differently in softwood and hardwood species:

$$\left\{ \begin{array}{l} \text{Hardwood: } \alpha = \frac{\sigma_{TW} + \sigma_{NW}}{2}; \beta = \frac{\sigma_{TW} - \sigma_{NW}}{2} \\ \text{Softwood: } \alpha = \frac{\sigma_{CW} + \sigma_{NW}}{2}; \beta = \frac{\sigma_{NW} - \sigma_{CW}}{2} \end{array} \right. \quad (10a)$$

$$\left\{ \begin{array}{l} \text{Hardwood: } \alpha = \frac{\sigma_{TW} + \sigma_{NW}}{2}; \beta = \frac{\sigma_{TW} - \sigma_{NW}}{2} \\ \text{Softwood: } \alpha = \frac{\sigma_{CW} + \sigma_{NW}}{2}; \beta = \frac{\sigma_{NW} - \sigma_{CW}}{2} \end{array} \right. \quad (10b)$$

σ_{TW} (resp. σ_{CW}) being the maturation stress in the [tension wood TW](#) (resp. [compression wood CW](#)), and σ_{NW} that in the opposite wood ([NW](#)). One gets :

$$\left\{ \begin{array}{l} \delta F_0 = -\pi R (2\alpha + e\beta) \delta R + \delta N \\ \delta F_1 = -\pi R^2 (3\alpha e + e^2\beta + \beta) \delta R - \delta M \end{array} \right. \quad (11a)$$

$$\left\{ \begin{array}{l} \delta F_0 = -\pi R (2\alpha + e\beta) \delta R + \delta N \\ \delta F_1 = -\pi R^2 (3\alpha e + e^2\beta + \beta) \delta R - \delta M \end{array} \right. \quad (11b)$$

140 From equations (8), (11a) and (11b), the components of the system (7) are known. By inversion, $\delta\alpha$ and
141 δb can be obtained according to the following equations (see details in Appendix B):

$$\left\{ \begin{array}{l} \delta a = \frac{4}{ER} \left[\left(3e\bar{e} - 2e^2 - \frac{1}{2} \right) \alpha + \left(\bar{e}e^2 - e\bar{e}^2 + \bar{e} - \frac{e}{4} \right) \beta \right] \delta R + \frac{4}{E\pi R^3} \left[\bar{e}\delta M + \left(\bar{e}^2 + \frac{1}{4} \right) R\delta N \right] \\ \delta b = \frac{-4}{ER^2} \left[(3e - 2\bar{e}) \alpha + (e^2 - e\bar{e} + 1) \beta \right] \delta R - \frac{4}{E\pi R^4} (\delta M + \bar{e}R\delta N) \end{array} \right. \quad (12a)$$

$$\left\{ \begin{array}{l} \delta a = \frac{4}{ER} \left[\left(3e\bar{e} - 2e^2 - \frac{1}{2} \right) \alpha + \left(\bar{e}e^2 - e\bar{e}^2 + \bar{e} - \frac{e}{4} \right) \beta \right] \delta R + \frac{4}{E\pi R^3} \left[\bar{e}\delta M + \left(\bar{e}^2 + \frac{1}{4} \right) R\delta N \right] \\ \delta b = \frac{-4}{ER^2} \left[(3e - 2\bar{e}) \alpha + (e^2 - e\bar{e} + 1) \beta \right] \delta R - \frac{4}{E\pi R^4} (\delta M + \bar{e}R\delta N) \end{array} \right. \quad (12b)$$

142 Once δa and δb are known, the stress increment $\delta\sigma$ at any position given by (x', y') can be obtained from
143 equation(6). The stress distribution at this position can be obtained as the sum of the initial maturation
144 stress and all the stress increments undergone by the material point since its creation.

$$\sigma(x', y', R) = \sigma_0(x', y') + \sum_{k=k_{x'y'}}^K \delta\sigma_k \quad (13)$$

145 where $\delta R_k = r_k - r_{k-1}$ for a succession of ring radii $0 < r_0 < \dots < r_k < \dots < r_K = R$, $\delta\sigma_k$ is the
146 corresponding increment, and $k_{x'y'}$ designates the ring containing the point.

147 Analytical formulations

148 Using equations (12b) and dividing by δR , we get the following equations when δR tends to zero :

$$\left\{ \begin{array}{l} \frac{da}{dR} = \frac{4}{ER} \left[\left(3e\bar{e} - 2e^2 - \frac{1}{2} \right) \alpha + \left(\bar{e}e^2 - e\bar{e}^2 + \bar{e} - \frac{e}{4} \right) \beta + \frac{1}{\pi R^2} \left(\bar{e} \frac{dM}{dR} + \left(\bar{e}^2 + \frac{1}{4} \right) R \frac{dN}{dR} \right) \right] \\ \frac{db}{dR} = \frac{-4}{ER^2} \left[(3e - 2\bar{e}) \alpha + (e^2 - e\bar{e} + 1) \beta + \frac{1}{\pi R^2} \left(\frac{dM}{dR} + \bar{e}R \frac{dN}{dR} \right) \right] \end{array} \right. \quad (14a)$$

$$\left\{ \begin{array}{l} \frac{da}{dR} = \frac{4}{ER} \left[\left(3e\bar{e} - 2e^2 - \frac{1}{2} \right) \alpha + \left(\bar{e}e^2 - e\bar{e}^2 + \bar{e} - \frac{e}{4} \right) \beta + \frac{1}{\pi R^2} \left(\bar{e} \frac{dM}{dR} + \left(\bar{e}^2 + \frac{1}{4} \right) R \frac{dN}{dR} \right) \right] \\ \frac{db}{dR} = \frac{-4}{ER^2} \left[(3e - 2\bar{e}) \alpha + (e^2 - e\bar{e} + 1) \beta + \frac{1}{\pi R^2} \left(\frac{dM}{dR} + \bar{e}R \frac{dN}{dR} \right) \right] \end{array} \right. \quad (14b)$$

149 Using equation (13) and dividing again by a vanishing δR , we obtain the following equation involving the
 150 partial derivative $\partial\sigma/\partial R$:

$$\sigma(x', y', R) = \sigma_0(x', y') + \int_{R_{x'y'}}^R \frac{\partial\sigma}{\partial R}(x', R') dR' \quad (15)$$

151 where $R_{x'y'}$ is the radius of the section at the instant of appearance of the point with coordinates (x', y') .

On the other hand, the expressions of axial force $N(R)$ and bending moment $M(R)$ are required to compute the evolution of the stress distribution in the cross section. For this purpose, we assumed that both vary as a power function of the radius of the branch. This resulted in the following allometric laws:

$$\begin{cases} N = \lambda_N R^{\nu_N} & (16a) \\ M = \lambda_M R^{\nu_M} & (16b) \end{cases}$$

152 where $\lambda_{N,M}$ and $\nu_{N,M}$ are allometric coefficients. The λ -coefficients are directly proportional to the weight
 153 of the branch part supported by the cross section (the branch itself and the other axes of higher orders).
 154 The ν -coefficients express the kinetics of the secondary growth: a small ν refers to an early secondary
 155 growth while a higher one refers to a later diameter increase.

156

The calculation of σ requires also the knowledge of the temporal variation of the curvature b . In order to simplify the analyses, we mainly studied stationary cases, i.e. we assumed that the branch maintains its orientation and remains straight. This assumption results in $\frac{db}{dR} = 0$. Physiologically, this equation expresses that the branch always compensates its weight increment at each deposition step of a new wood layer, corresponding to an additional weight. However, we can consider two cases for which the branch does not build up in a stationary way: i) the passive bending (under its own weight) case, and ii) the up-righting case (i.e. the action of maturation is stronger than the additional weight). In both cases, the resulting change in curvature has been modelled by Alm eras and Fournier (2009) and Alm eras et al. (2018). It can then be written as follows:

$$\begin{cases} \text{Up-righting:} & \frac{db}{dR} = -4 \frac{\beta}{ER^2} & (17a) \\ \text{Passive bending:} & \frac{db}{dR} = 4 \frac{\lambda_M \nu_M}{E\pi} R^{\nu_M-5} & (17b) \end{cases}$$

157 For the next computations, we used the following general law:

$$\frac{db}{dR} = \lambda_b R^{\nu_b} \quad (18)$$

158 As a remark, even if this equation bears some resemblance to (16), it does not express any notion of
 159 allometry and is used here only for convenience. Combining (14),(15),(16) and (18), the total stress can
 160 then be computed as:

$$\sigma^i(x', y', R) = \sigma_0^i(x', y') + S_1 \ln\left(\frac{R}{R_{x'y'}}\right) + \frac{S_2}{S_3} \left(R^{S_3} - R_{x'y'}^{S_3}\right) + \frac{S_4}{S_5} \left(R^{S_5} - R_{x'y'}^{S_5}\right) + \frac{S_6}{S_7} \left(R^{S_7} - R_{x'y'}^{S_7}\right) x' \quad (19)$$

161 where $S_1 = 4 \left[\left(3e\bar{e} - 2e^2 - \frac{1}{2}\right) \alpha + \left(\bar{e}e^2 - e\bar{e}^2 + \bar{e} - \frac{e}{4}\right) \beta \right]$ is driven by the maturation process, $S_2 =$
 162 $\frac{\lambda_N \nu_N}{\pi} \left(\bar{e}^2 + \frac{1}{4}\right)$, $S_3 = \nu_N - 2$, $S_4 = \frac{4}{\pi} \lambda_M \nu_M \bar{e}$ and $S_5 = \nu_M - 3$ by the branch loading (geometric evolution
 163 of the branch), $S_6 = E\lambda_b$ and $S_7 = \nu_b + 1$ by the branch orientation.

164 For each radius r , the remaining unknowns are the mean stress α , the differential stress β and the
 165 eccentricity e . Equation (14b) can be rewritten as:

$$(3e - 2\bar{e})\alpha + (e^2 - e\bar{e} + 1)\beta = \frac{-1}{\pi R^2} \left(\frac{dM}{dR} + \bar{e}R \frac{dN}{dR} \right) - E \frac{R^2}{4} \frac{db}{dR} \quad (20)$$

166 Thus by fixing two parameters, the third is directly determined. The maturation parameters α and β are
 167 determined by the maturation stress σ_{NW} in normal wood and σ_{TW} or σ_{CW} in reaction wood according
 168 to equation (10).

169 We considered two possible configurations for the simulations in [the](#) next section:

1. First, we applied a constant eccentricity (so that $\bar{e} = e$) and we fixed the stress level in the normal wood. In that case, the maturation stress of the reaction wood was given by equations (10):

$$\begin{cases} \sigma_{TW} = \frac{-2}{\pi R^2(1+e)} \left(\frac{dM}{dR} + eR \frac{dN}{dR} \right) + \sigma_{NW} \left(\frac{1-e}{1+e} \right) + \lambda_b \left(\frac{ER^2}{2(1+e)} \right) R^{\nu_b} & (21a) \\ \sigma_{CW} = \frac{2}{\pi R^2(1-e)} \left(\frac{dM}{dR} + eR \frac{dN}{dR} \right) + \sigma_{NW} \left(\frac{1+e}{1-e} \right) - \lambda_b \left(\frac{ER^2}{2(1-e)} \right) R^{\nu_b} & (21b) \end{cases}$$

2. Second, we fixed the maturation parameters and we observed how the eccentric growth could, or not, maintain the orientation of the branch. In this configuration, equation (20) became a two degrees equation in e that could be solved numerically.

173 In these two configurations, using data on the support allometries $\lambda_N, \lambda_M, \nu_M, \nu_N$, we can calculate the
 174 stress in the [reaction wood RW](#) and/or the eccentricity with different (λ_b, ν_b) , then deduce the growth
 175 stress profile in the section (eq. 19). In the next part, we see how the allometric coefficients can be
 176 obtained from data generated by growth model.

177 Realistic growth data

178 Tree architecture modelling

179 Numerical experiments were carried out using two reference models: [a softwood, maritime pine \(*P. pinaster*\)](#)
 180 [and a hardwood, wild cherry \(*P. avium*\)](#) ~~one softwood *Pinus pinaster* (pine) and one hardwood *Prunus*~~
 181 ~~*avium* (birch)~~ (Fig 2). Their growth follows the architectural model of Rauh [Hallé et al. (1978)]. This
 182 implies that the branching is rhythmic, the axes are monopodial and the branches are orthotropic. These
 183 digital trees were computed with [the](#) AmapSim software [Barczy et al. (2007)]. The input of this software
 184 are architectural parameters which were provided by observations and field studies: Coudurier et al. (1993)
 185 and Heuret et al. (2006) for [P. pinaster *Pinus pinaster*](#), Caraglio (1996) and Barthélémy et al. (2009) for
 186 [P. avium *Prunus avium*](#). The choice of these species was based on the availability of temperate species
 187 in [the](#) AmapSim database. The two trees were modelled over 50 years in open-growth conditions, which
 188 did not correspond to the same ontogenic stage of development, but allowed both trees to be considered
 189 mature. In the final state, the pine (resp. [cherry birch](#)) was 18,2 m (resp. 14,1 m) high. The diameter at
 190 the base was 40 cm for both species. The insertion height of the first branch was 14,3 m for pine and 4,6
 191 m for the birch. The branches of interest were the main branches; those that were directly attached to the
 192 trunk. In addition, only branches that were more than 20 years old ~~were have been~~ studied, so that they
 193 had a consistent loading history. Finally, 33 branches for the pine and 45 for the birch were selected. For
 194 each of the branch groups, the distributions of length L , radius r and insertion angle with the trunk θ are
 195 shown in Table 1.

Species	L_m (m)	r_m (m)	θ_m (°)
P. pinaster <i>Pinus pinaster</i>	5.3 ± 0.4	5.2 ± 0.3	70 ± 0.01
P. avium <i>Prunus avium</i>	7.9 ± 1.4	8.1 ± 0.7	80 ± 0.05

Table 1: Geometric distribution of branches of interest

197

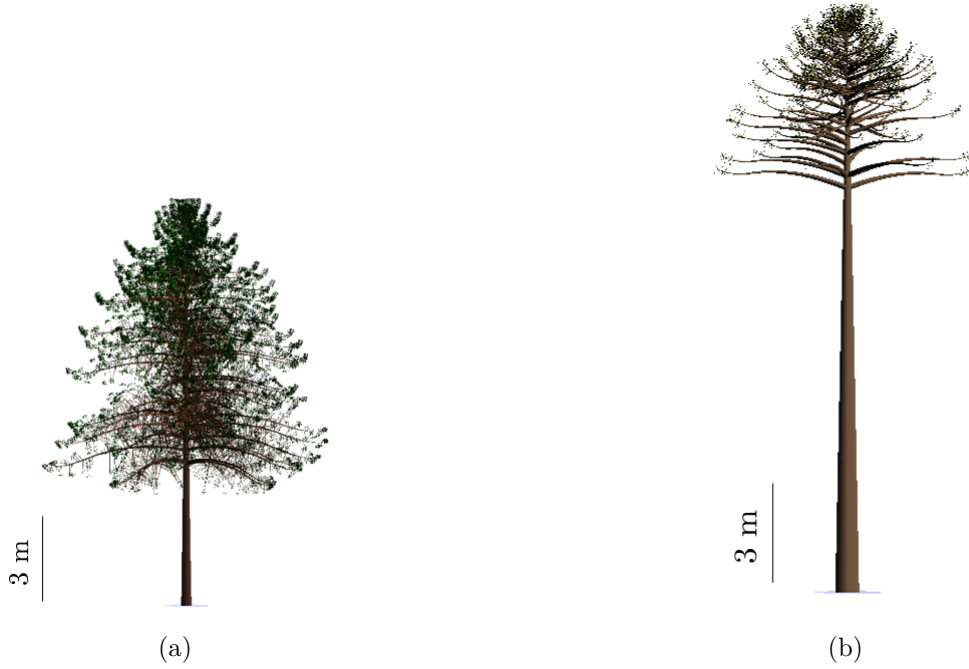


Figure 2: AmapSim representation of aerial architecture of 50-years old trees. (a) *Prunus avium* and (b) *Pinus pinaster*

198 **Loading scenarii: allometric laws**

199 Each tree was composed of axes organised hierarchically according to their order: 1 for the tree seed,
 200 2 for the trunk, 3 for the main branches, 4 for those attached to them, etc.. Each axis was described
 201 as a succession of growth units (GU), which were sections of cones, identified by a number (in order of
 202 appearance), and defined by a parent number, an order, a start and end diameter, the coordinates of the
 203 centres of both initial and final sections as well as their length (Fig 3). Note that the description provided
 204 by AmapSim did not include the internal structure of the growth units, such as eccentricity. To avoid
 205 unnecessary complications, the coordinates of the centres were taken as those of the pith. From the model
 206 data, the moments and normal forces can be computed in each growth unit, at any time of the tree's
 207 existence. In addition to a part of its own weight, each unit is subjected to the weight of its offsprings -
 208 this term referring to any growth unit that would fall if the studied one was cut. The normal force \vec{N}_n
 209 and bending moment \vec{M}_n supported by the growth unit n can be written:

$$\vec{N}_n = \frac{1}{2}m_n\vec{g} + \sum_{\substack{k>n \\ k \text{ offspring}}} m_k\vec{g} \quad (22)$$

$$\vec{M}_n = \overrightarrow{G_n G'_n} \wedge \left(\frac{1}{2}m_n\vec{g} \right) + \sum_{\substack{k>n \\ k \text{ offspring}}} \overrightarrow{G_n G_k} \wedge (m_k\vec{g}) \quad (23)$$

211 where G_n is the centre of gravity of the current growth unit, G'_n is the centre of gravity of its second half.
 212 On the downstream side of G_n , G_k is the centre of gravity of an offspring of number $k > n$, m_i is the mass
 213 of growth unit i and \vec{g} is the gravity vector. Once \vec{N}_n and \vec{M}_n were computed in the absolute coordinates
 214 used for the description of the whole tree, they were projected in the local coordinates system $(\vec{x}', \vec{y}', \vec{z})$,
 215 with \vec{z} of the chosen cross section. In the following, in accordance with the development of the previous
 216 section, N_z refers to the projection of \vec{N} on \vec{z} and M_y to the projection of \vec{M} on \vec{y}' .

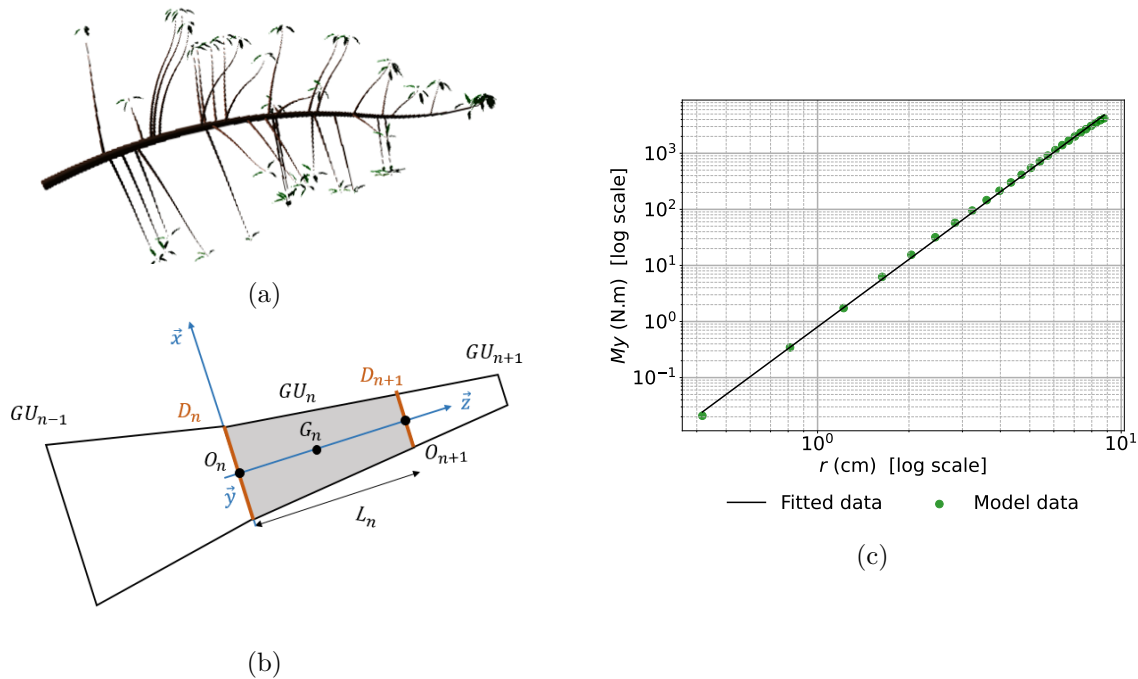


Figure 3: Illustration of the different steps of computation of the allometric law $M_y = f(r)$. First the modelled branch of *P. avium* (a) was divided into a succession of conical units (b). This allowed to compute the bending moment M . Then, the repetition of the computation each year, provided the relationship between the branch radius r and the bending moment M_y , represented in the graph (c). The fitted curve provides the final allometric law. Allometric law of *Prunus avium*. The bending moment is calculated from the geometry of the modelled branch (a) and (b). The graph (c) represents the relationship between the branch diameter and the bending moment. The fitted curve provides the allometric law.

217 Power law regressions were performed to recover the allometric coefficients $\lambda_M, \lambda_N, \nu_N, \nu_M$. A summary
 218 of the analysis process is proposed in Fig 3.

219 For the selected branch groups, the distribution of all allometric coefficients are presented in Fig 4. In *Pinus*,
 220 there was a large variation in ν -coefficient, with ν_M varying by almost a factor 2 in the studied sample;
 221 indicating very variable secondary growth kinetics. In *Prunus*, the range of variation of the allometric
 222 power coefficients was smaller, which depicted a higher homogeneity of secondary growth kinetics. For
 223 both species, a great diversity in λ -coefficients was observed, which depicted a significant variability
 224 in the loading history. This is particularly interesting as the branches showed geometric determinants
 225 that did not vary over large ranges (Table 1). Also, these coefficients do not appear to vary as a function
 226 of geometric parameters. This reflects the complexity of predicting the loading of a branch from the
 227 determinants of the main axis, and shows the importance of branching. In both cases, these variations in
 228 the λ -coefficients result in a factor of 4 in the bending load between the lightly loaded and the heavily
 229 loaded branches.

230 The average values of each allometric and final geometry, indicated in table 2, will be used for the
 231 simulations.

232 Material data

233 The stress values in the normal wood (NW) were fixed according to the average maturation strains advised
 234 by Thibaut and Gril (2021). Similarly, the green wood MOE were given by the correlation between dry
 235 and green MOE identified by Thibaut and Gril (2021): $E_g = 0.89 * E_d$. Dry MOE were provided by the

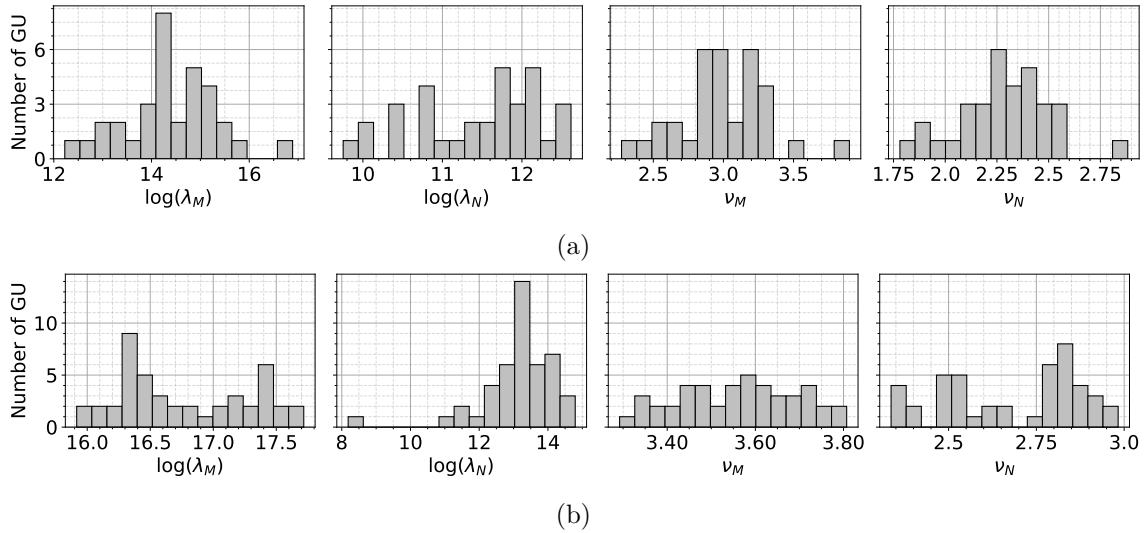


Figure 4: Statistical distribution of allometric coefficients for modelled branches: (a) *Pinus pinaster* (b) *Prunus avium*. $\lambda_{M,N}$: weight factor. $\nu_{M,N}$: kinetic of secondary growth factor. (See equation 16 for more details). ~~$\lambda_{M,N}$ refers to the weight, $\nu_{M,N}$ to the kinetic of secondary growth.~~

236 tropix database of CIRAD [Gérard et al. (2011)]. The density of green wood was approximated by the
 237 density of water $\rho = 1000 \text{ kg.m}^{-3}$. These inputs are summarised in Table 2.
 238 In the following section, the case of stationary growth ($\nu_b = 0$) will be considered principally and analysed
 239 thoroughly. Situations of changing curvature will be then considered briefly.

Species	λ_M	λ_N	ν_M	ν_N	r	μ_{NW}	E_d	E_g
<i>Pinus pinaster</i> / <i>Pinus pinæ</i>	-6.4e6	5e4	3.2	2.5	0.05	410	8.8	7.9
<i>Prunus avium</i>	-2.6e7	9.5e3	3.6	2.7	0.08	712	10.2	9.1

Table 2: Mean input characteristics of the branches. $\lambda_{N,M}$ and $\nu_{N,M}$ correspond to the allometric evolution of the normal load and bending moment, r (m) is the radius at the basal part of the branch, ν_{NW} (μ strain) is the maturation strain in the normal wood (NW), and $E_{d,g}$ (GPa) is the dry and green modulus of the material.

241 Results

242 *Prunus avium*

243 Fig 5 shows ~~the results of the simulations for *P. avium* simulation results obtained for *Prunus avium*,~~
 244 when one of the factors (eccentricity or reaction wood RW) is set to zero. On Fig 5.a, the stress on the
 245 whole section is represented. In this case, the branch maintains its orientation through the formation of
 246 reaction wood RW only (no eccentric growth). The area near the pith is under in compression (red), while
 247 the periphery is under in tension (blue), with a higher tension on the upper side, allowing to maintain the
 248 orientation. ~~The~~ Fig 5.b shows the interpolation of the stress distribution of Fig 5.a on the main axis $y=0$.
 249 Fig 5.c represents the maturation stress in the tension wood TW throughout the growth of the branch.
 250 ~~The larger the branch grew, the higher the needed stress level. This stress becomes greater as the branch~~
 251 grows. The symmetric case, with no formation of reaction wood RW but eccentric growth, is presented
 252 in Fig 5.d-f. This example illustrates that eccentricity alone could theoretically provide the orientation
 253 control. Fig 5.f shows the evolution of the eccentricity through the radial growth of the branch. Like the
 254 reaction wood RW stress in the previous case, the needed eccentricity increased when the branch grew.
 255 The pattern of stress distribution of Fig 5.d is quite similar to that a in in Fig 5.a , with compression near

256 the pith and tension at the periphery, but the section is off-centred and the tension at periphery is the
 257 same all around the section, confirming the absence of [reaction wood RW](#).

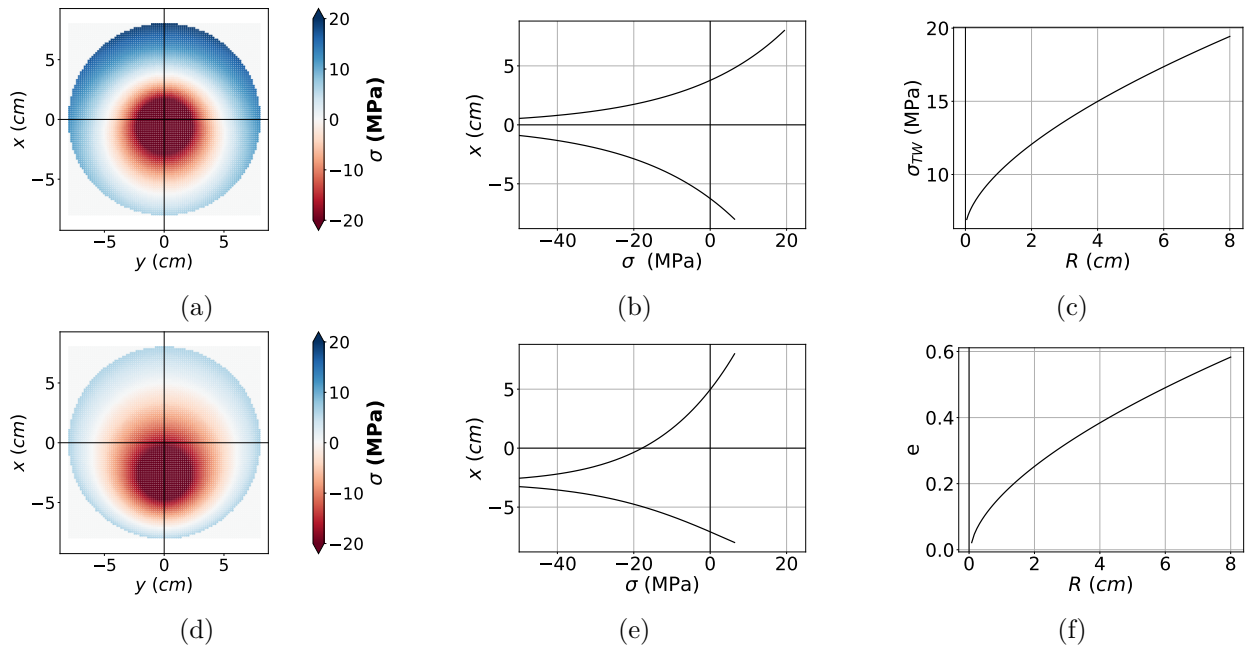
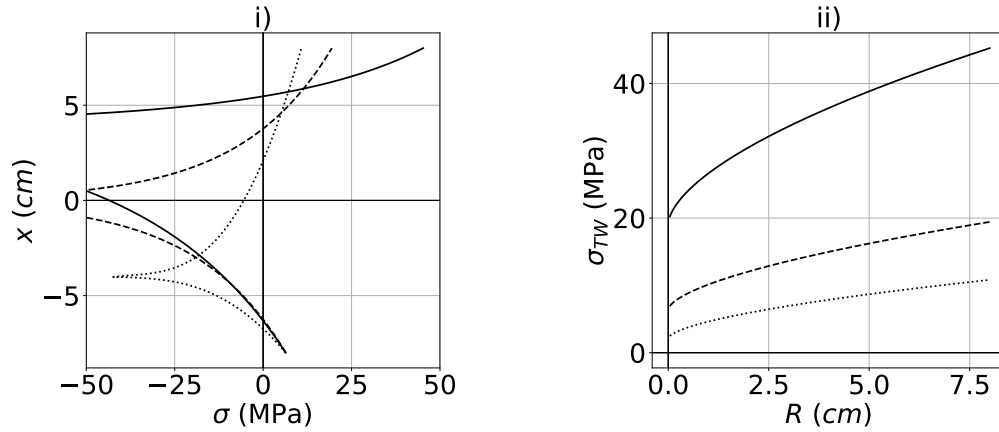


Figure 5: *Prunus avium*: The horizontal orientation of the branch is maintained by the two different processes: (a-c) the maturation stress provided by the formation of [reaction wood RW](#); (d-f) the eccentric growth; (a,d) 2D visualisation of the growth stress in the whole section; (b,e) Growth stress profile on diameter $y=0$. (c,f) Parametric representation of the tropic driver, maturation stress (c) and eccentricity (f).

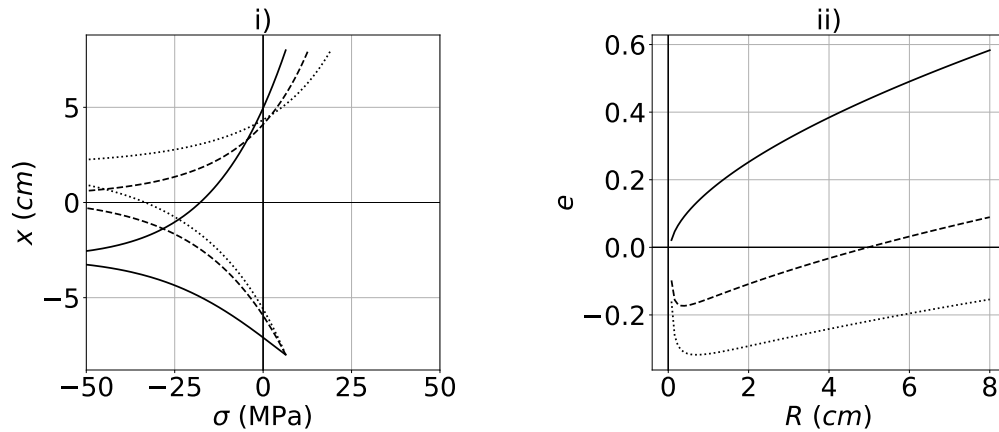
258 Fig 6 shows the combination of the two factors. For each of them, three different scenarii were proposed.
 259 In Fig 6.a, the [reaction wood RW](#) controlled the orientation. Different eccentricities, ranging from -0.5
 260 to 0.5 were imposed. The resulting stress patterns are represented in Fig 6.a.i : the higher tension on
 261 the upper side maintained the posture. ~~The more hypotrophic the eccentricity, the higher the tension~~
 262 ~~stress at periphery. This tension stress becomes higher as the eccentricity becomes hypotrophic.~~ This is
 263 confirmed by the evolution of the maturation stress induced by [reaction wood RW](#) through branch growth
 264 in Fig 6.a.ii. The situations where the eccentricity controlled the posture are shown in Fig. 6.b. Where
 265 uniform tension was imposed ($\sigma_{TW} = 2\sigma_{NW}$, $\sigma_{TW} = 3\sigma_{NW}$), the eccentricity pattern became particular:
 266 we observed a decrease during the first year, followed by an increase (Fig 6.b.ii). This is explained by
 267 the growth scenario: at the beginning of the development, fixing a uniform [reaction wood RW](#) formation
 268 tended to right-up the stem, while a stationary orientation was imposed. Therefore, the eccentricity process
 269 counteracted this righting up movement, leading to the initial decrease. As the branch grew, the effect of
 270 [reaction wood RW](#) decreased and the branch tended to bend forward: the eccentricity counteracted this
 271 trend, leading to the final increase. This coordination problem may probably be specific to our scenario
 272 that imposed a stationary orientation throughout the entire growth the branch, including the first stages
 273 of development.

274 *Pinus pinaster*

275 For *Pinus pinaster*, we used the same approach. The set of results is presented in Fig 7 and Fig 8. When
 276 no eccentricity was involved (Fig 7.a-c), a light compression stress was observed on the lower side of the
 277 section. When the branch grew, the compression stress increased (Fig 7.c). In case of no [reaction wood](#)
 278 [RW](#) formation (i.e. homogeneous maturation stress), the distributions of growth stress and eccentricity



(a) Stress in tension wood σ_{CW} is the main driver of postural control. Different eccentricities are applied : solid line, epitrophic eccentricity $e = -0.5$, dashed line, no eccentricity, $e = 0$ and dotted line, hypotrophic eccentricity $e = 0.5$.



(b) Eccentricity e is the main driver of postural control. Different maturation gradients $\sigma_{TW} - \sigma_{NW}$ are applied : solid line, no maturation gradient ($\sigma_{TW} = \sigma_{NW}$), dashed line, $\sigma_{TW} = 2\sigma_{NW}$ and dotted line $\sigma_{TW} = 3\sigma_{NW}$

Figure 6: Different possible options to maintain the orientation of *Prunus avium* branches: stress in reaction wood RW (a) or eccentricity (b). For each option, the subfigure (i) represents the total stress on diameter $y=0$, and the subfigure (ii) shows the evolution of the tropic driver (e or σ_{CW}) vs. the radius R of the branch each year. Different possible options to maintain the orientation of *Prunus avium* branches: (a) a constant eccentricity combined with the maturation that becomes the main driver of postural control; or (b) a constant maturation gradient combined with an eccentricity that becomes the main driver of postural control.

279 (Fig 7.d-f) were quite similar to the previous example with the birch tree: tension in periphery, compression
 280 near the pith, and an increasing eccentricity with branch growth.

281 The combination of the two factors is shown in Fig 8. As in for *Prunus avium*, different eccentricities were
 282 imposed (Fig 8.a): the more epitrophic the eccentricity, the higher reaction wood RW maturation stress.
 283 Although the different compression stress levels were close, the dynamic of this stress within the growth of
 284 the branch was different (Fig 8.a.ii). Also, the stress pattern exhibits a difference near the pith (Fig. 8.a.i),
 285 with some tension in this area for eccentricity $e = 0.5$. In case of a uniform reaction wood RW maturation
 286 (8.b), the profile remained quite similar to birch tree. We could not impose a too low compression stress
 287 because of the above-mentioned coordination incompatibility.

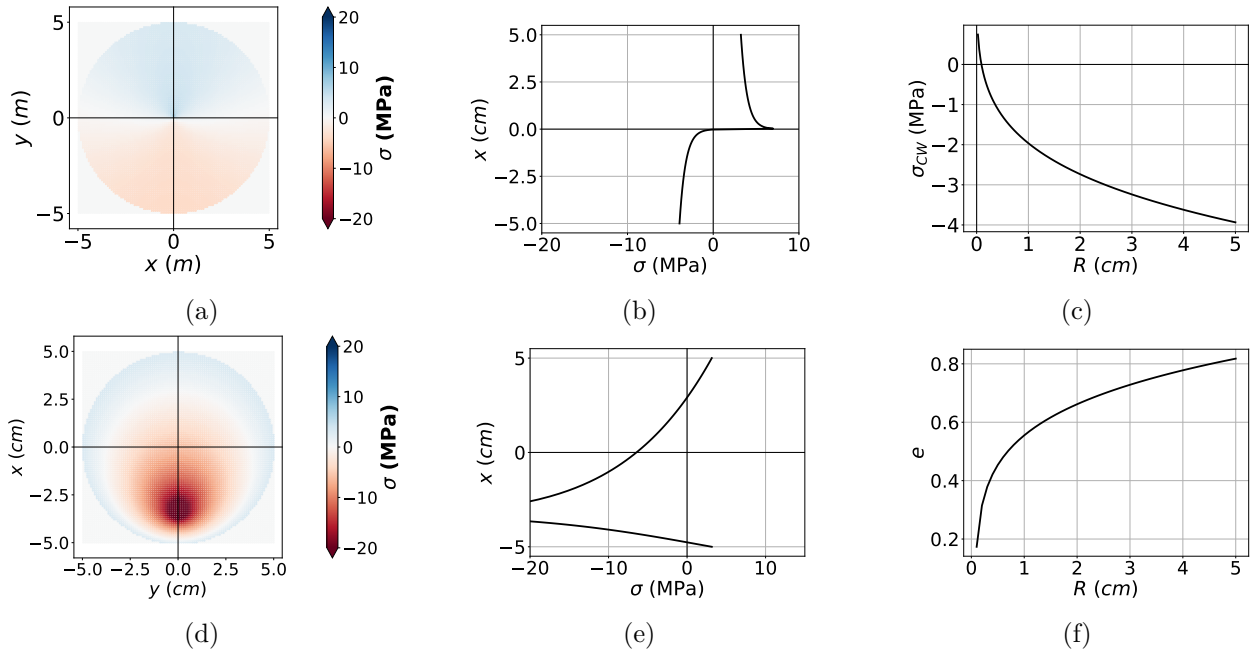
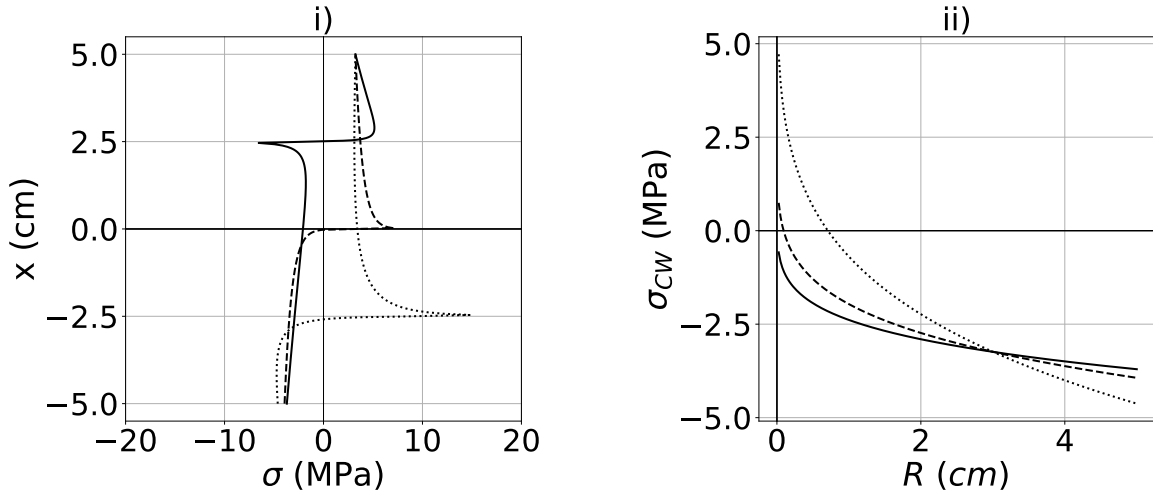


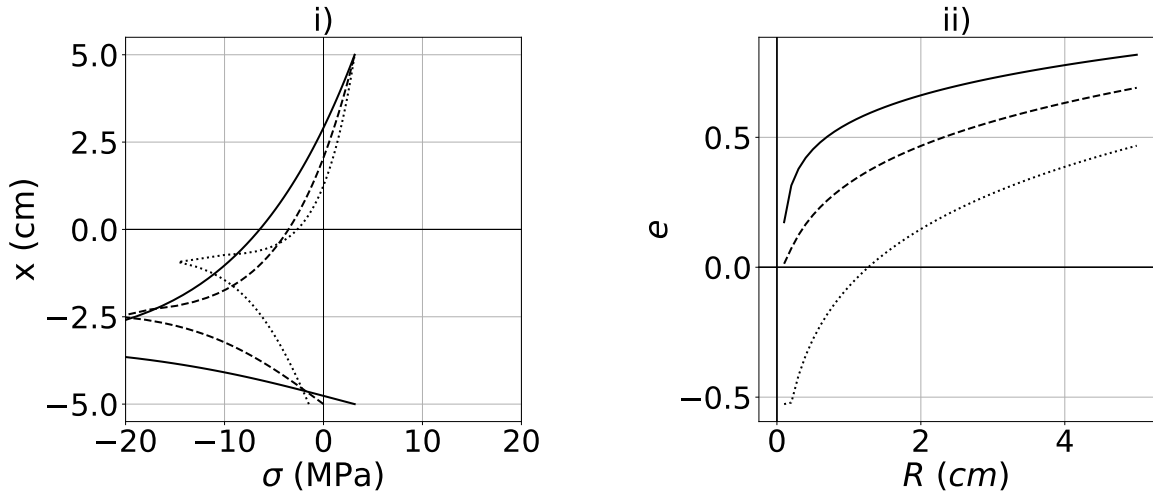
Figure 7: *Pinus pinaster*: The horizontal orientation of the branch is maintained by the two different processes: (a-c) the maturation stress provided by the formation of [reaction wood RW](#); (d-f) the eccentric growth; (a,d) 2D visualisation of the growth stress in the whole section; (b,e) Growth stress profile on diameter $y=0$. (c,f) Parametric representation of the tropic driver, maturation stress (c) and eccentricity (f).

288 Influence of branch orientation: the stationarity hypothesis

289 In order to evaluate the relevance of the stationarity hypothesis, i.e., the branch keeps the same orientation,
 290 different growth scenarii were considered. For each branch, the case of active up-righting or passive
 291 bending was modelled (using equation 17). Passive bending was driven by increasing weight, calculated
 292 on the modelled branches. Up-righting was driven by the maturation gradient, which was set at 400
 293 μ strain ($\sigma \approx 3.2$ MPa) for pine and 700 μ strain ($\sigma \approx 6.2$ MPa) for [cherry birch](#) (the gradient was of
 294 the order of magnitude of normal wood stress). The results are shown in Fig 9. In [cherry birch](#), no
 295 major change of the stress pattern was observed. In contrast, the pattern changed greatly for pine. For a
 296 passive-bending branch, a 'V' profile and the absence of compression wood were observed. For up-righting,
 297 the previously-mentioned profile with tension at the pith was observed.

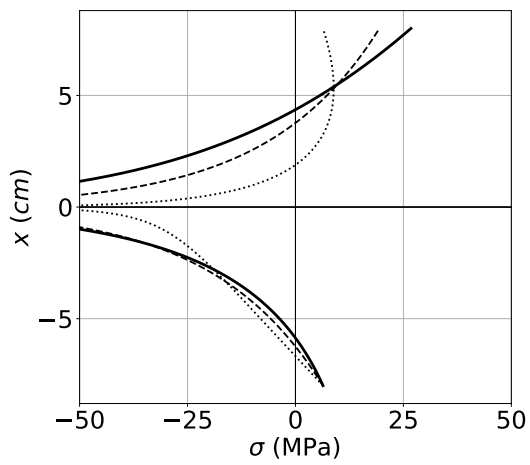


(a) Stress in compression wood σ_{CW} is the main driver of postural control. Different eccentricities are applied : solid line, epitrophic eccentricity $e = -0.5$, dashed line, no eccentricity, $e = 0$ and dotted line, hypotrophic eccentricity $e = 0.5$.

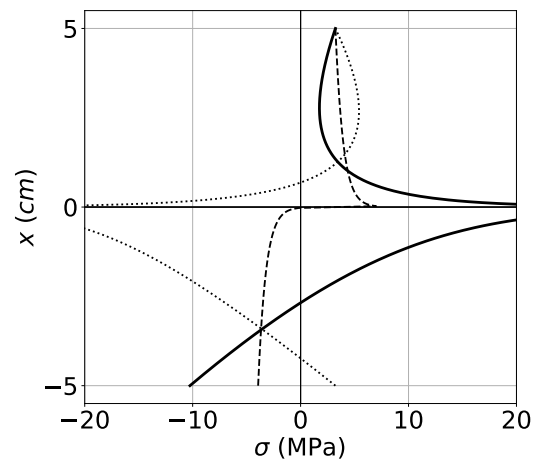


(b) Eccentricity e is the main driver of postural control. Different constant maturation gradients $\sigma_{NW} - \sigma_{CW}$ are applied : solid line, no maturation gradient ($\sigma_{NW} = \sigma_{CW}$), dashed line, $\sigma_{CW} = 0$. Dotted line is the maximal absolute value of σ_{CW} before divergence of the computation.

Figure 8: Different possible options to maintain the orientation of *Pinus pinaster* branches: stress in reaction wood RW (a) or eccentricity (b). For each option, the subfigure (i) represents the total stress on the diameter $y=0$, and the subfigure (ii) shows the evolution of the tropic driver (e or σ_{CW}) vs. the radius R of the branch each year. Different possible options to maintain the orientation of *Pinus pinaster* branches: (a) a constant eccentricity combined with the maturation that becomes the main driver of postural control; or (b) a constant maturation gradient combined with an eccentricity that becomes the main driver of postural control.



(a) Prunus



(b) Pinus

Figure 9: Distribution of growth stresses on diameter $y=0$ for different orientation scenarii. Solid line, up-righting movement; dashed line, stationarity; dotted line, passive bending.

Discussion

Prunus avium: heavily loaded hardwood

Regarding the stress distribution (Fig 5), using either eccentric growth or [reaction wood RW](#) formation led to realistic [stress values orders of magnitude](#) (except near the pith, which is an intrinsic limit of our model. This specific point is discussed in section *Limits of the model*). In the case with no eccentricity, a tensile strain of $\mu_{RW} \approx 2140\mu\text{strain}$ ($\sigma_{TW} \approx 19.5$ MPa) was obtained, quite similar to literature values, for much smaller branches: on 4 cm plagiotropic branches of eight tree species, Tsai et al. (2012) reported an average strain in [reaction wood RW](#) of around $2100\mu\text{strain}$, with some values up to $\approx 5000\mu\text{strain}$. When combined with uniform eccentricity (Fig 6.a), it seems safer to promote the growth on the upper side: it minimises both high tensile stress and area with high compression stress. Interestingly, the worst case (hypotrophic eccentricity $e = -0,5$, more, solid line in Fig 6.a) led to levels approaching the limits, but previously observed [Huang et al. (2005); Tsai et al. (2012)]: $\mu_{RW} \approx 4970\mu\text{strain}$ ($\sigma_{TW} \approx 45.4$ MPa)). Note that although for softwoods, there is a consensus on the usually observed eccentricity orientation (hypotrophic [Timell (1986)]), the eccentricity has been observed in both directions in hardwood branches [Kucera and Philipson (1977); Wang et al. (2009b); Tsai et al. (2012)] although not usually in [the](#) trunk. Therefore, this could be a tropic response for angiosperms branches, that tend to bend forward. This non-optimal pattern would be the consequence of a coordination between eccentricity and maturation stress. An extensive measurement campaign on branches would be needed to clarify this point. In the absence of [reaction wood RW](#) (Fig 5.d-f), the eccentricity alone ensured the orientation. The maximal value was around 0.6, ~~which corresponds to an average eccentricity of 0.35. Although the absolute value is realistic, average eccentric found in literature is on the opposite side.^{err}, which seems quite high compared to literature values.^{err}~~ For example, Hung et al. (2017) performed measurements on 10 plagiotropic branches of *Koelreuteria elegans* (Seem.) A.C.Sm. The average radius was 2.6 cm, and the [average^{err}](#) eccentricity had an average value of -0.37, with a maximum at -0.54. Unpublished data on more than 150 branches from six different temperate species showed very different patterns, depending from the species, but eccentricity was never below -0.5. ~~This suggests that eccentricity is a limited driver of postural control.^{err} This result suggests that eccentricity doesn't usually counteract gravity. Also the combination of radial growth eccentricity with uniform maturation stress showed the same tendency as the dual combination (uniform eccentricity): a higher maturation stress led to a larger eccentricity. Comparing all simulations, the most theoretical optimal case was a constant positive eccentricity (dotted line in Fig 6.a), which is again not what is showed by experimental observations. It raises interesting question on the main mechanical driver of branch construction. From a biological point a view, it could be less "costly" to produce tension wood than to produce a large amount of wood for an eccentricity result. But this hypothesis was never investigated. Also, more work is needed to understand how tension wood and eccentricity are linked in angiosperm trees: since they may have some uncoordinated action, we can wonder if they have common triggered factors.^{err}~~

~~Finally, these results suggest that growth eccentricity doesn't have the same role in branches and trunks: Alm eras et al. (2005) showed that eccentricity in leaning stems explains $\approx 29\%$ of the of the curvature!^{err} This result is in line with the work of Alm eras et al. (2005), who showed that eccentricity in leaning stem explains a much lower part of the curvature than the maturation gradient ($\approx 29\%$ for eccentricity while $\approx 66\%$ for maturation gradient)^{err}.~~

~~The combination of radial growth eccentricity with uniform maturation stress showed the same tendency as the dual combination (uniform eccentricity): a higher maturation stress led to a larger eccentricity. Comparing all simulations, the most optimal case was a constant positive eccentricity (dotted line in Fig 6.a). However, experimental observation showed that this is not the usual configuration for branches. It raises interesting question on the main mechanical driver of branch construction. From a biological point a view, it could be more "costless" to produce TW than eccentricity, but this hypothesis was not yet investigated. Also, more work is needed to understand how TW and eccentricity are linked in angiosperm~~

346 ~~trees: since they may have some uncoordinated action, we can wonder if they have common triggered~~
347 ~~factors.~~^{err}

348 *Pinus pinaster*: lightly loaded softwood

349 First of all, the values of the stress distribution were much lower than for *Prunus avium*. This was explained
350 by the size of the modelled branches: the average bending moment is much higher for ~~cherry birch~~
351 than for pine, by a factor of roughly 10 (see λ_M and λ_N in Table 2). The effect of each factor alone (Fig
352 7) suggested that maturation is a much more efficient option than eccentricity. To ensure the same growth
353 scenario, the eccentricity alone rose to about 0.8, which is close to a theoretical limit, whereas maturation
354 alone led to low maturation strains in compression wood CW ($<500 \mu\text{strain}$, corresponding to 4 MPa).
355 Besides, this eccentricity was not in the direction of what is commonly observed. This point remains
356 logical, because without compression wood, the epitrophic eccentricity is the only way to counteract the
357 effect of gravity.

358 A uniform eccentricity combined with reaction wood RW formation led to quite similar patterns (Fig 8.a):
359 for this range of loading, the eccentricity had little influence on stress distribution. Considering that the
360 density of elastic energy is proportional to the square of the stress, the pattern produced a low level of
361 stored elastic energy, possibly reducing the risk of mechanical failure. Also, although eccentricity did
362 not bring much variations in the value of the maturation stress, it considerably modified the shape of
363 the resulting stress profiles (Fig 8.a.i). Indeed, these profiles can become 'crenellated' (Fig 8.a.i, dashed
364 curve for zero eccentricity, solid curve for $e = -0.5$) or include tension at the pith (dotted line for
365 $e = 0.5$). It seems that before producing tension in the pith, an efficient configuration could be reached by
366 generating compression below the pith and tension above. Ideally, this may be a very relevant option for
367 branches. These results about the mechanical strategies of branches should be confronted to experimental
368 measurements. Otherwise, these pattern changes could also be an optimisation of the residual strength
369 of wood: compression wood CW is known to have high compressive strength conferred by its high lignin
370 content and cell wall structure. Generating some tension at the pith allows the branch to create more
371 compression wood CW. To answer this question it would be necessary to take into account strength
372 parameters in our stress computation model. Adding a damage-elastoplastic law would also allow to study
373 the effects of stress relaxation and to observe if some profiles, that are here not optimal for maintaining
374 the branch orientation, could possibly become optimal for resisting breakage.

375 Using eccentricity combined to formation (Fig 8.b) leads to usual patterns, with compression near the
376 pith, tension on the upper side and compression on the lower one. Eccentricity is epitrophic: this is the
377 opposite to what is usually observed: unpublished data on 20 branches (average radius of 3 cm) of *Pinus*
378 *nigra* showed an average eccentricity of -0.2. This non-intuitive result is partly explained by our hypothesis
379 of uniform stiffness, as will be discussed later. It is also explained here by the change of sign between
380 normal wood NW and compression wood CW. In the early stages of growth, as long as the stress in the
381 compression wood CW is lower than in the normal wood NW, the best option to maintain the orientation
382 is to do epitrophic eccentricity. Once the stress in the compression wood CW becomes higher than in the
383 normal wood NW, it is more efficient to do hypotrophic eccentricity. Our scenarios do not allow us to
384 reach stress levels in compression that are higher than the stress in normal wood NW. This is due to the
385 above mentioned incompatibility of our scenario.

386 Influence of branch orientation : the stationary hypothesis

387 In both trees, the orders of magnitude are compatible with a mechanical safety margin for the branches.
388 Apart from modified tropisms (change of light environment, weight change by loss of part of the branch,
389 etc.), the maintenance maintaining of the orientation is quite common for real branches. However our
390 simulations suggest that if, for any reason, branches need to modify their orientation, they can do it
391 without taking too much mechanical risk. ~~The hypothesis of branch direction stationarity is totally in~~
392 ~~accordance with the long-term mechanical requirements needed during the construction of branches.~~

393 Vertical bending moment vs horizontal bending and torsion moments

394 One of the [hypotheses hypothesis](#) of our model was that the vertical bending moment (M_y) prevails over
395 the torsional M_z and horizontal bending M_x moments. This allowed to consider only one direction of
396 eccentricity and to avoid all the non-linear terms generated by the torsional components. We evaluated the
397 maximum values of the three moments for all modelled branches of each species for comparison purpose.
398 The results are presented in Fig 10. They [show enlighten](#) that for each species, the vertical moment
399 [displays shows](#) much higher values than the torsional and horizontal bending moments and validates our
400 initial hypothesis.

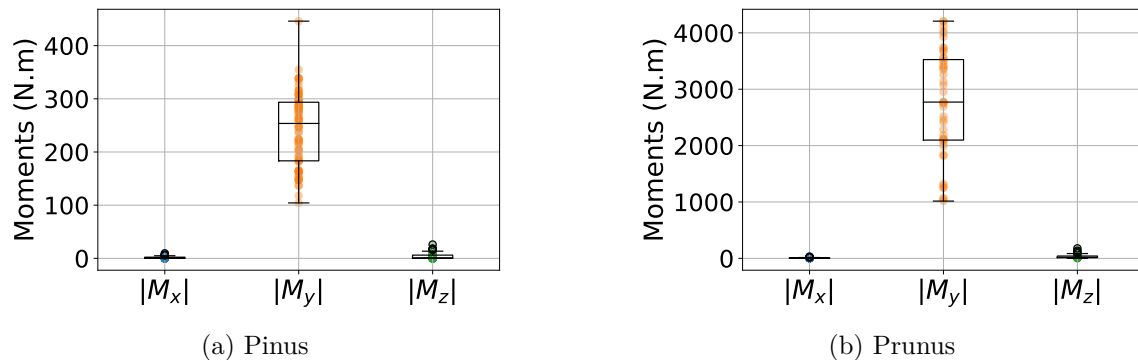


Figure 10: Comparison of maximum moments for [the branches modelled in this research modelled branches](#). M_x : horizontal moment; M_y : vertical moment; M_z : torsional moment.

401 Limits of the model

402 The hypothesis of homogeneous wood stiffness in the whole [branch](#) section is questionable. Systematic
403 stiffness differences have been observed between wood types ([tension wood TW](#) or [compression wood CW](#)
404 vs [normal wood NW](#)). Alm eras et al. (2005) have studied the variation of Young's modulus in the section
405 of leaning stems from 14 angiosperms and 3 gymnosperms, all coming from different families. For the
406 angiosperms, the average Young's modulus of tension wood was higher than in [normal wood NW](#) by 15%,
407 while for the gymnosperms, the Young's modulus was 38% lower in [compression wood CW](#) than in [normal](#)
408 [wood NW](#). This heterogeneity of rigidity plays a role in the postural control of the stems [Alm eras et al.
409 (2005); Huang et al. (2010); Hung et al. (2017)]. In our case, either a higher rigidity in tension wood or a
410 lower one in [compression wood CW](#) would make the branch bend upward. In the current formulation of
411 the model imposing an homogeneous stiffness, an almost equivalent effect would have been obtained by
412 an initial offset in the eccentricity. Calling this offset tentatively 'compensating eccentricity' e_c (Fig 11),
413 the model computed a total eccentricity, e , combining e_c and the "real" eccentricity needed to maintain
414 the orientation. Therefore, in case in formation on one side, the eccentricity displayed needs to be offset
415 by e_c to correspond to more realistic situations. This explains, for instance, why the simulations for the
416 softwood resulted in hypertrophic eccentricity while it is well-known that inclined softwood stems usually
417 exhibit hypotropic eccentricity. Although data are missing to approximate the value of this parameter,
418 and further work is needed to assess theoretically the possible equivalence between rigidity variations
419 and eccentricity, the available information on relative stiffness of [normal wood NW](#) and suggests a more
420 important effect in gymnosperms than in angiosperms.

421 The evaluation of the stress during the first stages of branch development is another issue of the model. In
422 almost every stress profile, a tension or compression peak is generated in the pith. It generally exceeds the
423 wood strength, which is not compatible with branch sustainability. This point could be corrected in two
424 ways. First, the role of the bark could be taken into account. Its importance in postural maintenance was
425 clearly highlighted [Clair et al. (2019); Ghislain et al. (2019)]. Our model could include the mechanical

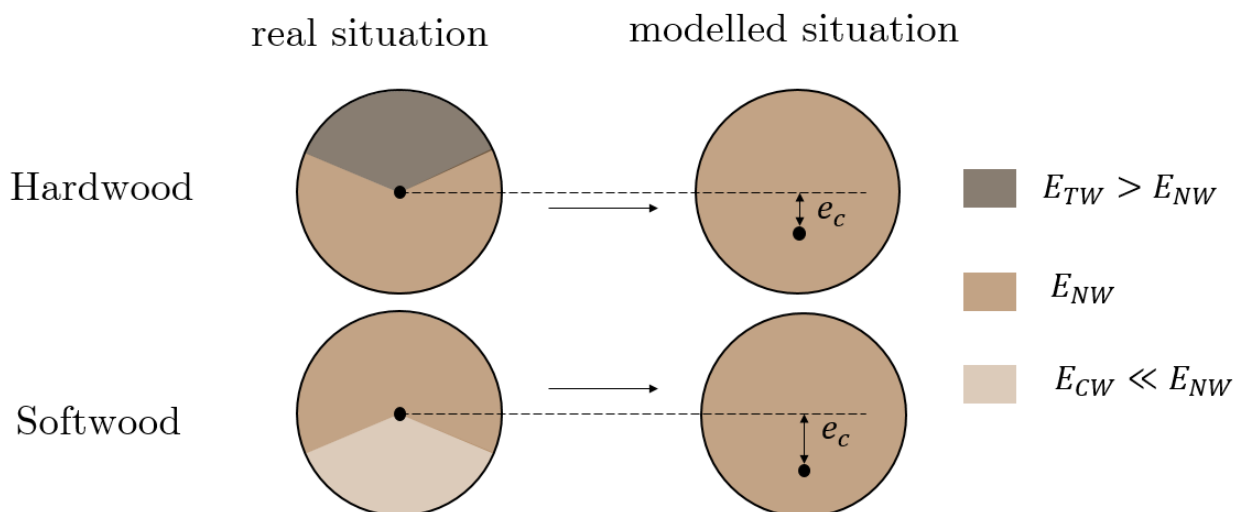


Figure 11: How the hypothesis of a uniform wood stiffness impacts the initial position of the pith. [ec](#): pith offset equivalent to a centered pith with heterogenous wood properties; [E_{TW}](#), [E_{NW}](#), [E_{CW}](#): Longitudinal Young’s modulus of tension, normal, compression wood, respectively.

426 action of bark in the early stages of branch development. This improvement would require additional data
 427 about the mechanical behaviour of the bark but would bring more realistic stress predictions and limit
 428 the artefacts at the pith. A second exciting perspective would be to take into account the elastoplastic
 429 behaviour of wood. By imposing a realistic plastic strain limit, the peak at the pith would then disappear;
 430 the increments would be spread over the middle part of the section, thus modifying the non-realistic
 431 patterns previously observed.

432 Finally, modelling the evolution of normal force and bending moment loads by allometric laws remains
 433 questionable. Indeed, the orientation of the branch may vary with time, which implies variations of the
 434 effect of weight. For example, modelling a constant increase of the normal force is inappropriate if the
 435 inclination of the branch decreases with time. An improvement of our model could be the construction
 436 of loads based on equivalent length allometries taking into account the mass of the branch, and the
 437 computation of the loads for each position in the right reference frame.

438 Conclusion and perspectives

439 A semi-analytical growth stress model has been developed in the context of branch development. [This](#)
 440 [model was applied to test the effectiveness of two well-known biomechanical processes of woody plants](#)
 441 [to control the orientation of their axes: eccentric radial growth and formation. At each radius increment,](#)
 442 [the stress balance is computed in order to fit with a observed curvature. A first novelty of this model is](#)
 443 [that it takes into account the role of the eccentricity variation over the years. A second contribution is the](#)
 444 [computation of stress distribution in the whole cross-section. We tested the effectiveness of two well-known](#)
 445 [biomechanical processes of woody plants to control the orientation of their axes: eccentric radial growth](#)
 446 [and formation. The case of a softwood \(*Pinus pinaster* Aiton\) and a hardwood \(*Prunus avium* L\) were](#)
 447 [computed using data provided by the AmapSim software. For both trees, growth stress simulations showed](#)
 448 [that maturation stress was more efficient than eccentric radial growth to maintain a fixed orientation \(i.e.](#)
 449 [to counter the increasing gravity constrain applied to the growing branch\).For the hardwood branches,](#)
 450 the computations highlighted that the eccentricity needed to maintain orientation did not corroborate the
 451 observations reported in literature. This suggests that this parameter probably provides another function
 452 than the orientation control, like the improved bending strength of the branch that provides it a greater
 453 mechanical safety. For the softwood branches, although the model showed that eccentric radial growth

454 did not play a major role in maintaining the branch’s orientation, it does modify the shape of the stress
 455 profiles in the cross section of the branch. A few odd and critical profiles, crenellated or with tension near
 456 the pith, have been identified. Their analysis provided exciting perspectives for further experimental works
 457 to gather real data.

458 Now that a complete model is available, it becomes crucial to start experimental investigations on branches
 459 in order to compare the outputs with real in situ observations. Especially, we need to evaluate the relevance
 460 of the different biological processes used by branches to ensure their mechanical sustainability over the
 461 years.

462 From a biological point of view, a key point for understanding branch sizing is the question of biomass
 463 costs. Building additional wood on one side or forming are carbon sinks with possible trade-offs. In
 464 order to investigate this point, our model could help by affecting a cost to the production of as well as to
 465 eccentric growth. The resulting computations could then help to understand the relevance of some options
 466 and would lead to coupling the biomechanical point of view to other biological considerations.

467 References

- 468 T. Alméras, D. Jullien, and J. Gril. *Modelling, Evaluation and Biomechanical Consequences of Growth Stress*
 469 *Profiles Inside Tree Stems*, pages 21–48. Springer International Publishing, Cham, 2018. ISBN 978-3-319-
 470 79099-2. doi: 10.1007/978-3-319-79099-2_2. URL https://doi.org/10.1007/978-3-319-79099-2_2.
- 471 T. Alméras and B. Clair. Critical review on the mechanisms of maturation stress generation in trees.
 472 *Journal of The Royal Society Interface*, 13(122):20160550, 2016. doi: 10.1098/rsif.2016.0550. URL
 473 <https://royalsocietypublishing.org/doi/abs/10.1098/rsif.2016.0550>.
- 474 T. Alméras and M. Fournier. Biomechanical design and long-term stability of trees: Morphological and
 475 wood traits involved in the balance between weight increase and the gravitropic reaction. *Journal of*
 476 *Theoretical Biology*, 256(3):370–381, 2009. ISSN 0022-5193. URL [http://www.sciencedirect.com/
 477 science/article/pii/S0022519308005389](http://www.sciencedirect.com/science/article/pii/S0022519308005389).
- 478 T. Alméras, A. Thibaut, and J. Gril. Effect of circumferential heterogeneity of wood maturation strain,
 479 modulus of elasticity and radial growth on the regulation of stem orientation in trees. *Trees*, 19(4):
 480 457–467, 2005. ISSN 1432-2285. URL <https://doi.org/10.1007/s00468-005-0407-6>.
- 481 P. Ancelin, T. Fourcaud, and P. Lac. Modelling the biomechanical behaviour of growing trees at the forest
 482 stand scale. part i: Development of an incremental transfer matrix method and application to simplified
 483 tree structures. *Annals of Forest Science*, 61(3):263–275, 2004.
- 484 R. R. Archer. On the distribution of tree growth stresses. ii. stresses due to asymmetric growth strains.
 485 *Wood Science and Technology*, V10:293–309, 1976.
- 486 R. R. Archer and F. E. Byrnes. On the distribution of tree growth stresses – part i: An anisotropic
 487 plane strain theory. *Wood Science and Technology*, 8(3):184–196, 1974. ISSN 1432-5225. URL
 488 <https://doi.org/10.1007/BF00352022>.
- 489 J.-F. Barczy, H. Rey, Y. Caraglio, P. de Reffye, D. Barthélémy, Q. X. Dong, and T. Fourcaud. AmapSim:
 490 A Structural Whole-plant Simulator Based on Botanical Knowledge and Designed to Host External
 491 Functional Models. *Annals of Botany*, 101(8):1125–1138, 09 2007. ISSN 0305-7364. doi: 10.1093/aob/
 492 mcm194. URL <https://doi.org/10.1093/aob/mcm194>.
- 493 D. Barthélémy, Y. Caraglio, and S. Sabatier. 4.1 crown architecture of valuable broadleaved species.
 494 *Valuable broadleaved forests in Europe*, 22:87, 2009.

- 495 D. Barthélémy and Y. Caraglio. Plant Architecture: A Dynamic, Multilevel and Comprehensive Approach
496 to Plant Form, Structure and Ontogeny. *Annals of Botany*, 99(3):375–407, 01 2007. ISSN 0305-7364.
497 doi: 10.1093/aob/mcl260. URL <https://doi.org/10.1093/aob/mcl260>.
- 498 Y. Caraglio. Le développement architectural du merisier. *Forêt Entreprise* 107, (107):72–80, 1996.
- 499 B. Clair, B. Ghislain, J. Prunier, R. Lehnebach, J. Beauchêne, and T. Alméras. Mechanical contribution
500 of secondary phloem to postural control in trees: the bark side of the force. *New Phytologist*, 221(1):
501 209–217, 2019. doi: <https://doi.org/10.1111/nph.15375>. URL <https://nph.onlinelibrary.wiley.com/doi/abs/10.1111/nph.15375>.
- 502
- 503 T. Coudurier, D. Barthelemy, B. Chanson, F. Courdier, and C. Loup. Premier résultats sur la modélisation
504 du pin maritime pinus pinaster ait.(pinaceae). *Architecture des arbres fruitiers et forestiers*, page 306,
505 1993.
- 506 C. Coutand, M. Fournier, and B. Moulia. The gravitropic response of poplar trunks: Key roles of
507 prestressed wood regulation and the relative kinetics of cambial growth versus wood maturation.
508 *Plant Physiology*, 144(2):1166–1180, 2007. ISSN 0032-0889. doi: 10.1104/pp.106.088153. URL <http://www.plantphysiol.org/content/144/2/1166>.
- 509
- 510 J. B. Fisher and J. W. Stevenson. Occurrence of reaction wood in branches of dicotyledons and its
511 role in tree architecture. *Botanical Gazette*, 142(1):82–95, 1981. doi: 10.1086/337199. URL <https://doi.org/10.1086/337199>.
- 512
- 513 T. Fourcaud, F. Blaise, P. Lac, P. Castéra, and P. de Reffye. Numerical modelling of shape regulation and
514 growth stresses in trees. *Trees*, 17(1):31–39, 2003. ISSN 1432-2285. URL <https://doi.org/10.1007/s00468-002-0203-5>.
- 515
- 516 M. Fournier, B. Chanson, D. Guitard, and B. Thibault. Mécanique de l’arbre sur pied : modélisation d’une
517 structure en croissance soumise à des chargements permanents et évolutifs. 1. analyse des contraintes de
518 support. 1991a.
- 519 M. Fournier, B. Chanson, D. Guitard, and B. Thibault. Mécanique de l’arbre sur pied : modélisation d’une
520 structure en croissance soumise à des chargements permanents et évolutifs. 2. analyse tridimensionnelle
521 des contraintes de maturation, cas du feuillu standard. 1991b.
- 522 M. Fournier, H. Baillères, and B. Chanson. Tree biomechanics : growth, cumulative prestresses, and
523 reorientations. *Biomimetics*, 2(3):229–251, 1994.
- 524 B. Ghislain, T. Alméras, J. Prunier, and B. Clair. Contributions of bark and tension wood and role of the
525 g-layer lignification in the gravitropic movements of 21 tropical tree species. *Annals of Forest Science*,
526 76(4):107, 2019. ISSN 1297-966X. URL <https://doi.org/10.1007/s13595-019-0899-7>.
- 527 J. Gérard, D. Guibal, S. Paradis, M. Vernay, J. Beauchêne, L. Brancheriau, I. Châlon, C. Daigremont,
528 P. Détienne, D. Fouquet, P. Langbour, S. Lotte, M.-F. Thévenon, C. Méjean, and A. Thibaut. *Tropix* 7,
529 2011. URL <http://tropix.cirad.fr/en>.
- 530 F. Hallé, R. A. Oldeman, and P. B. Tomlinson. *Tropical trees and forests: an architectural analysis*.
531 Springer Verlag, 1978.
- 532 P. Heuret, C. Meredieu, T. Coudurier, F. Courdier, and D. Barthélémy. Ontogenetic trends in the
533 morphological features of main stem annual shoots of pinus pinaster (pinaceae). *American Journal of*
534 *Botany*, 93(11):1577–1587, 2006. doi: <https://doi.org/10.3732/ajb.93.11.1577>. URL <https://bsapubs.onlinelibrary.wiley.com/doi/abs/10.3732/ajb.93.11.1577>.
- 535
- 536 Y.-S. Huang, S.-S. Chen, L.-L. Kuo-Huang, and C.-M. Lee. Growth strain in the trunk and branches of

- 537 chamaecypris formosensis and its influence on tree form. *Tree Physiol*, 25(9):1119–1126, Sept. 2005.
538 ISSN 0829-318X. URL <https://doi.org/10.1093/treephys/25.9.1119>.
- 539 Y.-S. Huang, L.-F. Hung, and L.-L. Kuo-Huang. Biomechanical modeling of gravitropic response of
540 branches: roles of asymmetric periphery growth strain versus self-weight bending effect. *Trees*, 24(6):
541 1151–1161, 2010. ISSN 1432-2285. URL <https://doi.org/10.1007/s00468-010-0491-0>.
- 542 L.-F. Hung, C.-C. Tsai, S.-J. Chen, Y.-S. Huang, and L.-L. Kuo-Huang. Study of tension wood in
543 the artificially inclined seedlings of koelreuteria henryi dummer and its biomechanical function of
544 negative gravitropism. *Trees*, 30(3):609–625, 2016. ISSN 1432-2285. URL <https://doi.org/10.1007/s00468-015-1304-2>.
- 545
- 546 L.-F. Hung, C.-C. Tsai, S.-J. Chen, Y.-S. Huang, and L.-L. Kuo-Huang. Strain distribution, growth
547 eccentricity, and tension wood distribution in the plagiotropic and orthotropic branches of koelreuteria
548 henryi dummer. *Trees*, 31(1):149–164, 2017. ISSN 1432-2285. URL <https://doi.org/10.1007/s00468-016-1464-8>.
- 549
- 550 L. J. Kucera and W. R. Philipson. Growth eccentricity and reaction anatomy in branchwood of drimys
551 winteri and five native new zealand trees. *New Zealand Journal of Botany*, 15(3):517–524, 1977. doi:
552 10.1080/0028825X.1977.10429625. URL <https://doi.org/10.1080/0028825X.1977.10429625>.
- 553 H. Kübler. Studien über wachstumsspannungen des holzes iii. längenänderungen bei der wärmebehandlung
554 frischen holzes. *Holz Rohst Werkst*, 17(3):77–86, 1959.
- 555 J. E. Nicholson. A rapid method for estimating longitudinal growth stresses in logs. *Wood Science and*
556 *Technology*, 5(1):40–48, 1971. ISSN 1432-5225. URL <https://doi.org/10.1007/BF00363119>.
- 557 B. Thibaut. Three-dimensional printing, muscles, and skeleton: mechanical functions of living wood.
558 *Journal of Experimental Botany*, 70(14):3453–3466, 04 2019. ISSN 0022-0957. doi: 10.1093/jxb/erz153.
559 URL <https://doi.org/10.1093/jxb/erz153>.
- 560 B. Thibaut and J. Gril. Tree growth forces and wood properties. *Peer Community Journal*, 1:e46, 2021. doi:
561 10.24072/pcjournal.48. URL [https://peercommunityjournal.org/articles/10.24072/pcjournal.](https://peercommunityjournal.org/articles/10.24072/pcjournal.48/)
562 [48/](https://peercommunityjournal.org/articles/10.24072/pcjournal.48/).
- 563 T. E. Timell. *Compression wood in gymnosperms*, volume 1. Springer, 1986.
- 564 C.-C. Tsai, L.-F. Hung, C.-T. Chien, S.-J. Chen, Y.-S. Huang, and L.-L. Kuo-Huang. Biomechanical
565 features of eccentric cambial growth and reaction wood formation in broadleaf tree branches. *Trees*, 26
566 (5):1585–1595, 2012. ISSN 1432-2285. URL <https://doi.org/10.1007/s00468-012-0733-4>.
- 567 Y. Wang, J. Gril, and J. Sugiyama. Variation in xylem formation of viburnum odoratissimum var. awabuki:
568 growth strain and related anatomical features of branches exhibiting unusual eccentric growth. *Tree*
569 *Physiol*, 29(5):707–713, May 2009a. ISSN 0829-318X. URL <https://doi.org/10.1093/treephys/tpp007>.
- 570
- 571 Y. Wang, J. Gril, and J. Sugiyama. Is the branch of viburnum odoratissimum var. awabuki reaction
572 wood? unusual eccentric growth and various distributions of growth strain. In *6th Plant Biomechanics*
573 *Conference*, pages 328–334, 2009b.
- 574 H. Yamamoto, M. Yoshida, and T. Okuyama. Growth stress controls negative gravitropism in woody
575 plant stems. *Planta*, 216(2):280–292, 2002. ISSN 1432-2048. URL <https://doi.org/10.1007/s00425-002-0846-x>.
- 576
- 577 J. L. Yang, H. Baillères, T. Okuyama, A. Muneri, and G. Downes. Measurement methods for longitudinal
578 surface strain in trees: a review. *Australian Forestry*, 68(1):34–43, 2005. doi: 10.1080/00049158.2005.
579 10676224. URL <https://doi.org/10.1080/00049158.2005.10676224>.

580 M. Yoshida and T. Okuyama.: Techniques for measuring growth stress on the xylem surface using strain
581 and dial gauges. 56(5):461–467, 2002. doi: doi:10.1515/HF.2002.071. URL [https://doi.org/10.1515/
582 HF.2002.071](https://doi.org/10.1515/HF.2002.071).

583 **Appendix A**

584 The calculation of integrals of system (3) requires preliminary elements. The situation of two consecutive
 585 rings is represented in Fig. 12. Each position x in the geometrical reference frame is expressed with respect
 586 to the position x' in the pith reference frame according to the equation:

$$x = r \cos \theta = x' - \bar{e}R \quad (24)$$

with r the radius at time t and R the radius at the final time.

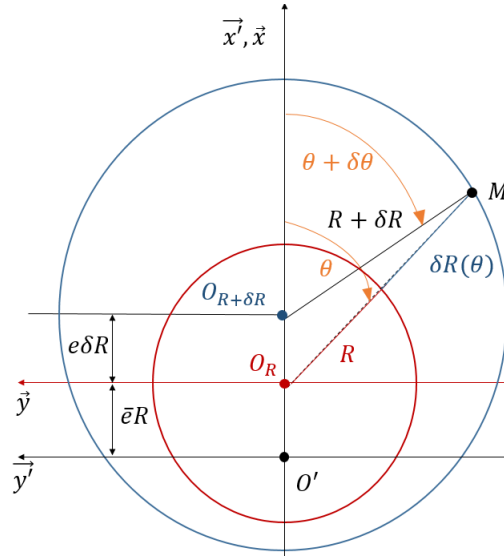


Figure 12: Representation of two consecutive rings and the elements needed to calculate $\delta R(\theta)$

587

588 The integrals of system (3) are computed as follows:

$$\begin{aligned} \int_s \delta \sigma ds &= \int_s E [\delta a + (x + \bar{e}.R)\delta b] r \delta r d\theta \\ &= E\pi R^2 (\delta a + \bar{e}.R\delta b) \\ \int_s x' \delta \sigma ds &= \int_s [\delta a + (x + \bar{e}.R)\delta b] [x + \bar{e}.R] r \delta r d\theta \\ &= E\pi R^3 \left[\bar{e}\delta a + R \left(\bar{e}^2 + \frac{1}{4} \right) \delta b \right] \end{aligned}$$

The tangential distribution of the radius increment $\delta R(\theta)$ is required to compute the maturation terms. Applying $\overrightarrow{O_R M} - \overrightarrow{O_{R+dR} M} = \overrightarrow{O_R O_{R+dR}}$ (Fig 12):

$$\begin{cases} [R + \delta R(\theta)] \cos \theta - (R + \delta R) \cos (\theta + \delta \theta) = e_R \delta R & (25a) \\ [R + \delta R(\theta)] \sin \theta - (R + \delta R) \sin (\theta + \delta \theta) = 0 & (25b) \end{cases}$$

589 By setting $\delta \theta \rightarrow 0$, it comes:

$$\begin{cases} \cos (\theta + \delta \theta) = \cos \theta - \sin \theta \delta \theta & (26a) \\ \sin (\theta + \delta \theta) = \sin \theta + \cos \theta \delta \theta & (26b) \end{cases}$$

590 Substituting (26) into (25), and combining (25a) and (25b), $\delta R(\theta)$ can finally be written as:

$$\boxed{\delta R(\theta) = \delta R [1 + e_R \cos \theta]} \quad (27)$$

Then:

$$\begin{aligned} \int_{\delta s} \sigma_0^i ds &= \int_{\delta s} \sigma_0^i(\theta) R \delta R(\theta) d\theta \\ &= \int_{\delta s} [\alpha + \beta \cos \theta] [1 + e \cos \theta] R \delta R(\theta) d\theta \\ &= \pi (2\alpha + e\beta) R \delta R \\ \int_{\delta s} x' \sigma_0^i ds &= \int_{\delta s} \sigma_0^i(\theta) (x + e.R) R \delta R(\theta) d\theta \\ &= R^2 \delta R \pi (3\alpha e + \beta e^2 + \beta) \end{aligned}$$

591 Appendix B

The matrix system (7) becomes:

$$\begin{cases} \delta a = \frac{\delta F_0 K_2 - \delta F_1 K_1}{K_0 K_2 - K_1^2} & (28a) \\ \delta b = \frac{\delta F_0 K_1 - \delta F_1 K_0}{K_1^2 - K_0 K_2} & (28b) \end{cases}$$

592 Then, numerators and denominators are calculated separately:

$$K_0 K_2 - K_1^2 = E^2 \pi^2 R^6 \left(\bar{e}^2 + \frac{1}{4} \right) - E^2 \pi^2 R^6 \bar{e}^2 = \frac{(E \pi R^3)^2}{4}$$

$$\begin{aligned} \delta F_0 K_2 - \delta F_1 K_1 &= E \pi^2 R^5 \left[-(2\alpha + e\beta) \left(\bar{e}^2 + \frac{1}{4} \right) + \bar{e} (3\alpha e + \beta e^2 + \beta) \right] \delta R + E \pi R^3 \left[R \delta N \left(\bar{e}^2 + \frac{1}{4} \right) + \bar{e} \delta M \right] \\ &= E \pi^2 R^5 \left[\alpha \left(3e\bar{e} - 2\bar{e}^2 - \frac{1}{2} \right) + \beta \left(\bar{e}e^2 - e\bar{e}^2 + \bar{e} - \frac{e}{4} \right) \right] \delta R + E \pi R^3 \left[R \delta N \left(\bar{e}^2 + \frac{1}{4} \right) + \bar{e} \delta M \right] \end{aligned}$$

$$\begin{aligned} \delta F_0 K_1 - \delta F_1 K_0 &= E \pi^2 R^4 \left[-\bar{e} (2\alpha + e\beta) + (3\alpha e + e^2 \beta + \beta) \right] \delta R + E \pi R^2 [\bar{e} R \delta N + \delta M] \\ &= E \pi^2 R^4 \left[\alpha (3e - 2\bar{e}) + \beta (1 + e^2 - e\bar{e}) \right] \delta R + E \pi R^2 [\bar{e} R \delta N + \delta M] \end{aligned}$$

Putting the calculations together, system (28) becomes:

$$\begin{cases} \delta a = \frac{4}{ER} \left[\alpha \left(3e\bar{e} - 2\bar{e}^2 - \frac{1}{2} \right) + \beta \left(\bar{e}e^2 - e\bar{e}^2 + \bar{e} - \frac{e}{4} \right) \right] \delta R + \frac{4}{E\pi R^3} \left[R \delta N \left(\bar{e}^2 + \frac{1}{4} \right) + \bar{e} \delta M \right] \\ \delta b = \frac{-4}{ER^2} \left[\alpha (3e - 2\bar{e}) + \beta (1 + e^2 - e\bar{e}) \right] \delta R + \frac{-4}{E\pi R^4} [\bar{e} R \delta N + \delta M] \end{cases}$$

593 Appendix C

594 The following calculus is based on Fig 3.b. To get the vertical bending moment M_y of unit n (eq 23), one
 595 need the calculation of each volume V_n and center of gravity G_n . Let name $D(z)$ the diametral extension
 596 of the cone. It comes:

$$V_n = \int_0^{L_n} \frac{\pi D(z)^2}{4} dz \quad (30)$$

597 where $D(z) = D_n + \left(\frac{D_{n+1}-D_n}{L_n}\right)z$. One gives

$$O_n G_n = \frac{1}{V_n} \int_0^{L_n} \frac{\pi D(z)^2}{4} z dz \quad (31)$$

Setting $\gamma = \frac{D_{n+1}-D_n}{D_n}$ and $\xi = \frac{L_n}{z}$, equations (30) and (31) become:

$$V_n = \frac{\pi D_n^2 L_n}{4} \int_0^1 (1 + \gamma \xi)^2 d\xi = \frac{\pi D_n^2 L_n}{4} \cdot \left(1 + \gamma + \frac{\gamma^2}{3}\right)$$

$$O_n G_n = \frac{1}{V_n} \frac{\pi D_n^2 L_n^2}{4} \cdot \left(\frac{1}{2} + \frac{2\gamma}{3} + \frac{\gamma^2}{4}\right)$$

598 So, finally, $O_n G_n$ can be written:

$$O_n G_n = \frac{L_n}{2} \left(\frac{1 + \frac{4}{3}\gamma + \frac{1}{2}\gamma^2}{1 + \gamma + \frac{1}{3}\gamma^2} \right) \quad (32)$$